Theory of negative corona in oxygen

R. Morrow
Division of Applied Physics, Commonwealth Scientific and Industrial Research Organization, Lindfield, Sydney, New South Wales 2070, Australia
(Received 13 November 1984)

Theoretical predictions are given of the development of the current and the distributions of charge and electric field in negative corona, or Trichel current pulses [G. W. Trichel, Phys. Rev. **54**, 1078 (1938)], in oxygen at a pressure of 6.67 kPa (50 Torr). For a 10-mm-diam negative sphere located 20 mm from a positive plane, the calculated current pulse has a rise time of 11 ns, a pulse width of 50 ns, and a peak amplitude of 13 mA. These results agree satisfactorily with experimental values. The predicted velocity of the cathode-directed light pulse also agrees well with observations. The theory is based on the accurate numerical solution of Poisson's equation in conjunction with the continuity equations for electrons, positive ions, and negative ions. The effects of ionization, attachment, recombination, electron diffusion, and photoemission and ion secondary-electron emission from the cathode are all included. The initial steep rise of the current pulse is largely due to rapid ionization and electron motion in the high Laplacian field near the cathode. As the discharge develops, a dense plasma forms near the cathode, leading to strong space-charge distortion of the field. A prominent cathode fall region is formed immediately adjacent to the cathode, an almost zero field is formed within the plasma and the field is enhanced over the region to the anode. The current pulse is quenched because the low electric field in the plasma immobilizes the majority of the electrons which then undergo three-body attachment; furthermore, the cathode fall region becomes reduced to such a short distance that insignificant current is produced from this region. Because of the low mobility of the negative ions, the current remains low and the structure of the space-charge fields changes only slowly with time between pulses.

I. INTRODUCTION

When an appropriate negative voltage is applied to the point of a point-plane electrode system in an electronegative gas, a pulsating corona current is observed in the external circuit. The current waveform consists of pulses having a very fast rise time and short duration, with a long period of relatively low current between the pulses. In oxygen (and air) the pulses are extremely regular and are called Trichel pulses,[1] after Trichel, who first reported the phenomenon.[2] In the pure SF_6, similar pulses occur, but they are irregular.[3] In nonattaching gases such as pure nitrogen, only a continuous corona current without pulses is observed.[1] Reviews of experimental results pertaining to negative corona have been presented by Loeb,[1] Sigmond,[4] and Goldman and Goldman.[5]

This paper presents a numerical study of the spatiotemporal development of electrons and positive and negative ions in space-charge-affected inhomogeneous electric fields. Although previous studies have considered some of the phenomena covered by this paper,[6–9] none has offered an integrated, quantitative theory.

Trichel himself argued that "the periodic character of the discharge seems to derive logically from space-charge formation in the gap and subsequent clearing under the action of the electrostatic field."[2] He predicted the build-up of a strong negative space charge away from the point and positive space charge near the point. "The presence of this cloud of positive ions in the gap at first causes a greatly increased field near the negative point...at the same time, the field beyond this space charge in the gap is decreased so that almost no ionization can take place." He postulated that the region of enhanced field near the cathode would become too narrow to sustain the discharge, and that ionization would consequently cease. Thus Trichel visualized many of the features of the Trichel pulse mechanism outlined below.

Loeb[1,10,11] presented a theory involving successive electron avalanches, each giving rise to three successors near the end of its development. The theory, however, failed to explain the fast rise time of 1.5 ns observed in air at atmospheric pressures[12] and the rapid quenching of the pulse.

Aleksandrov[6] extended Loeb's theory by considering the parallel development of many avalanches, rather than insisting on successive avalanches. He thus succeeded in predicting much faster rise times for the main pulse. He also predicted an initial phase of relatively slowly rising current before the main pulse, which was subsequently observed by Bugge and Sigmond.[13,14] The principle of Aleksandrov's approach is embodied in our continuity equations.

Khalifa and Abdel-Salaam,[15] Thanh,[16] and Graf[7] have also produced semiquantitative theories based on simulation models and not the equations of electron and ion continuity. Similarly, Kekez *et al.*,[17] described the point-plane discharge in terms of equivalent circuits and succeeded in describing a succession of pulses. However, the

model offers little insight into the detailed mechanisms of pulse formation. Dancer *et al.*[18] claim to provide a "unified theory" which draws together the experimental and theoretical evidence pertaining to Trichel pulses. However, their theory is not consistent with the results presented here, as outlined in the discussion (Sec. IV).

Ogasawara[19] has obtained analytic solutions describing the early current growth when the space-charge distortion of the Laplacian field is slight. However, Ogasawara's theory cannot describe the current waveform beyond its initial rise as an exponential current growth is assumed, and it cannot describe in detail the role of negative ions during the later stages of the discharge.

Davies and Donne[8] solved the one-dimensional continuity equations using a nonuniform mesh, and the method of moments to solve Poisson's equation. They obtained good agreement with the Trichel pulse shape measured in CO_2 by Gardiner and Craggs.[20] However, their calculations differ significantly from the present work in that (a) their peak current is 0.5 mA instead of 12 mA, (b) their maximum charge densities are 6×10^{9} cm^{-3} instead of 4×10^{11} cm^{-3}, and (c) no plasma region develops in front of the cathode with a well-defined and contracting cathode fall region as in the present calculations.

The present model is a development of earlier work by Morrow and Lowke,[21] Morrow,[22] and Morrow and Cram.[23,24] Preliminary results were presented by Morrow and Lowke,[9] who described a solution of the continuity equations in one dimension on a uniform mesh. Their predicted Trichel-pulse current waveform was in fair agreement with the results of Bugge[13] and the motion of the ions after the pulse gave a satisfactory explanation of the pulse frequency. However, the uniform mesh used in these early calculations did not adequately resolve phenomena at the cathode, and the results are therefore not quantitatively reliable.

Section II presents the general theory of the calculations, including the basic equations in Sec. II A and the numerical techniques in Sec. II B. The results are presented in Sec. III; a detailed description of the space-time development of the corona burst is presented in Sec. III A, while the different roles played by photons, attachment, and diffusion in the discharge are discussed in Secs. III B, III C, and III D, respectively. The results are discussed in Sec. IV, and the main conclusions of the study are presented in Sec. V. Appendix A contains the numerical treatment of the transport coefficients. Appendix B contains additional stability criteria. Finally Appendix C contains the details of the variable mesh.

II. THEORY

A. Basic equations

It is known from observation that the Trichel-pulse corona discharge occupies a cylindrical volume near the cathode. While it would be desirable to eventually develop a two-dimensional model to describe this system, computational constraints have led us to first consider a one-dimensional model in which continuity equations are used to describe only the axial development of the discharge. We expect that ambipolar diffusion in the radial direction will act to confine the discharge so that its radial development will be of secondary importance. Although one-dimensional continuity equations are used, we do account for the finite radius of the discharge in solving Poisson's equation for the distribution of axial electric field.

It is assumed that the material functions of the gas (such as drift velocity and ionization coefficients) are determined entirely by the local reduced electric field, E/N, where E is the electric field and N is the neutral gas number density. Lowke and Davies[25] have introduced the concept of an "equilibrium distance" ($d_{\rm eq}=D/W_e$) to test whether such local control obtains. According to this test, if E is reasonably constant over a distance of the order of $d_{\rm eq}$, the equilibrium coefficients should be adequate. An application of this test showed that the equilibrium assumption was valid throughout the discharge at most times. The formulas used to represent the transport coefficients are presented in Appendix A.

The continuity equations for electrons, positive ions, and negative ions in one-dimensional form, including ionization, attachment, recombination, and electron diffusion are

$$\frac{\partial N_e}{\partial t}=N_e\alpha\,|\,W_e\,|-N_e\eta\,|\,W_e\,|-N_eN_p\beta-\frac{\partial(N_eW_e)}{\partial x}+\frac{\partial^2(DN_e)}{\partial x^2}\,, \tag{1}$$

$$\frac{\partial N_p}{\partial t}=N_e\alpha\,|\,W_e\,|-N_eN_p\beta-N_nN_p\beta-\frac{\partial(N_pW_p)}{\partial x}\,, \tag{2}$$

$$\frac{\partial N_n}{\partial t}=N_e\eta\,|\,W_\epsilon\,|-N_nN_p\beta-\frac{\partial(N_nW_n)}{\partial x}\,. \tag{3}$$

Here t is time, x is distance from the cathode, N_e, N_p, and N_n are the electron, positive-ion, and negative-ion densities, respectively, and W_e, W_p, and W_n are electron, positive-ion, and negative-ion drift velocities, respectively. The material functions α, η, β, and D are, respectively, the ionization, attachment, recombination, and electron-diffusion coefficients. The continuity equations are coupled to Poisson's equation via the charge density.

As discussed by Davies and Evans[26] it is important to solve Poisson's equation in three dimensions to allow for the finite radial extent of the charge distribution. Thus the axial electric field $E(x)$ is evaluated using the method of disks[27] which represents the discharge as a cylinder with a uniform radial distribution and variable axial distribution of charge. In such a model the axial component of the electric field at point x is given by

$$E(x)=\frac{1}{2\epsilon_0}\left[\int_{-x}^{0}\rho(x+x')[-1-x'(x'^2+r^2)^{-1/2}]dx'+\int_{0}^{d-x}\rho(x+x')[1-x'(x'^2+r^2)^{-1/2}]dx'\right], \tag{4}$$

where $\rho(x)$ is the net charge density at x, r is the cylinder radius, and the gap extends from $x=0$ to d. In applying this equation, the electrode boundary conditions are implemented by including "images" of the charge $\rho(x)$ reflected appropriately at the surfaces of the perfectly conducting electrodes.[9] Morrow and Cram[23] show how Eq. (4) may be accurately represented by a simple operator which, because it depends only on the electrode geometry, is computed only once.

The initial Laplacian electric field is that due to a sphere-plane electrode pair, with a succession of appropriate image charges in the sphere and plane electrodes.[28] The Laplacian field is normalized to give the required voltage using

$$V_A=\int_0^d E_L dx \ , \tag{5}$$

where V_A is the applied voltage, E_L the Laplacian field, and d the electrode spacing. The space-charge field is added algebraically to the initial Laplacian field to give the resultant field in the gap.

The continuity equation for electrons, Eq. (1), is second order and therefore requires two boundary conditions. At the anode ($x=d$), we set $N_e=0$. At the cathode we set

$$N_e(x=0)=N_e^p+N_e^i \ , \tag{6}$$

where N_e^p is the number of secondary electrons released by photons and N_e^i the number of secondary electrons released by ions. The number of photoelectrons emitted at time t is[29]

$$N_e^p(0,t)=\frac{1}{|W_e(0,t)|}\frac{\gamma_p}{\tau}\int_0^t \exp\left[-\frac{t-t'}{\tau}\right]\int_0^d N_e(x,t')\,|W_e(x,t')|\,\alpha^*(x,t')\Omega(x)\exp(-\mu x)\,dx\,dt' \ . \tag{7}$$

Here, for the excited state considered μ is the coefficient of absorption, τ the lifetime, α^* the excitation coefficient, and γ_p the efficiency factor for release of photoelectrons at the cathode. The quantity $\Omega(x)$ is the solid angle subtended at the cathode by the disk of charge at x. The number of ion secondary electrons emitted at time t is given by

$$N_e^i(0,t)=\gamma_i\frac{N_i(0,t)\,|W_i(0,t)|}{W_e(0,t)} \ , \tag{8}$$

where γ_i is the ion—secondary-emission coefficient.

The continuity equations for positive and negative ions, Eqs. (2) and (3), are both first order and thus require only one boundary condition each. We set $N_n(x=0)=0$ and $N_p(x=d)=0$. At absorbing boundaries the heavy particle densities are finite and determined by the flux from the body of the discharge as discussed in Appendix B.

The current I in the external circuit due to the motion of electrons and ions between the electrodes is calculated using Sato's[30] equation, modified to include negative ions and electron diffusion:

$$I=\frac{\pi r^2 e}{V_A}\int_0^d\left[N_p W_p-N_n W_n-N_e W_e+\frac{\partial(DN_e)}{\partial x}\right]E_L\,dx \ . \tag{9}$$

Here V_A is the applied voltage and e the electron charge.

It will prove useful to discuss different phases of the discharge in terms of the replenishment criterion,[16]

$$\gamma_p\int_0^d\Omega(x)\alpha(x)\exp\left[\int_0^x[\alpha(x')-\eta(x')]dx'\right]dx\geq 1 \ . \tag{10}$$

This is an equilibrium criterion which determines the possibility of a self-sustained discharge occurring for a *given* field distribution. The criterion is applicable provided that the field changes slowly compared with the transit time of electrons through the ionization region. Ion secondaries are not included in the criterion because ions do not reach the cathode in significant numbers until well after the current rise and fall (cf. Fig. 5). In this case it is photons which supply the secondary electrons to make the pulse discharge current self-sustained. However, in a sense the discharge is self-sustained over long periods of time since the pulses repeat continuously without an external source of secondary electrons, and it is shown below that ions can provide the secondary electrons for this longer time-scale process.

It is assumed that ϕ, the light emitted by the discharge at any position, is proportional to the ionization activity[31] given as follows:

$$\phi(x,t)=N_e(x,t)\alpha(x,t)\,|W_e(x,t)| \ . \tag{11}$$

B. Numerical techniques

The simultaneous Eqs. (1)—(4) were solved numerically on a nonuniform mesh which had very fine spatial resolution in the cathode fall region, while grading to coarse but adequate resolution near the anode. On this nonuniform mesh, the convective and diffusive terms in Eqs. (1)—(3), were computed using the explicit flux-corrected-transport (FCT) algorithm and other techniques described by Morrow and Cram.[23,24] Further details of the numerical methods are included in Appendix B.

The time step taken for the computations must be limited by the simultaneous action of the Courant-Friedricks-Lewy condition

$$\Delta t\leq\frac{\Delta x}{|W_e|} \ , \tag{12}$$

and the von Neuman condition

$$\Delta t\leq\frac{\Delta x^2}{2D} \ . \tag{13}$$

It has been found useful to further limit the time step so that the relative change in the electric field in one time step is everywhere less than 10%. The time step is con-

tinuously adjusted to stay at 75% of the minimum step defined by the above limits. The calculations presented here use 76 000 time steps to follow the discharge for 213 ns.

The cathode is a 10-mm sphere with its center 25 mm from an infinite-plane anode. The electrode gap is thus 20 mm and the surface of the sphere nearest the plane is defined as the position $x=0$. A nonuniform mesh is defined along the axis of symmetry of this system as the set

$$x_i = x_{i-1} + \delta x_i \quad (i=2,3,\ldots,181) . \tag{14}$$

The variation in δx_i is summarized in Appendix C. The discharge is considered to be an 8-mm-diam cylinder centered on the axis of symmetry of this system.

The accuracy and robustness of the numerical techniques used in this paper have been extensively tested by Morrow and Lowke,[21] Morrow,[22] and Morrow and Cram.[23,24] Tests included halving the time step, which made an insignificant difference to the results, and halving the number of mesh points, which left all results negligibly altered except for minor changes in the current waveform after $t=70$ ns. This was due to lack of resolution of the cathode fall and plasma regions on the coarser mesh. Charge conservation was monitored by comparing the net charge inflow and outflow at the boundaries, integrated over time, with the net charge integrated over the discharge gap, at a given time. Charge was conserved to 0.005%. The net charge in the gap was always negative because of the release of secondary electrons from the cathode.

III. RESULTS

A. Space-time development of the corona burst

The calculation was initiated at $t=0$ ns by the release of 400 seed electrons at $x=55$ μm. The applied voltage was -2900 V. The computed current in the external circuit is presented in Fig. 1. After an initial slow growth, the current rises sharply, increasing from 10% to 90% of its peak value (~ 13 mA) in 11 ns. The pulse width at $\frac{1}{3}$ of the pulse amplitude is ~ 50 ns. Although the results presented here describe the first 213 ns of the discharge, extension of the calculations to 1300 ns showed a slow and continuing decay of the current to 0.04 mA. It is convenient and appropriate to divide our discussion in terms of *discharge phases* as defined by the letters (A–F) in Fig. 1.

1. Current multiplication in the Poisson-field phase

During the "current multiplication in the Poisson field phase," from $t=0$ to 26 ns (A to B in Fig. 1), electron multiplication is the dominant process. There are no space-charge or negative-ion effects. The discharge current grows slowly as predicted by Aleksandrov[6] and observed by Bugge and Sigmond.[13,14] At the end of this phase, $t=26$ ns, space-charge effects have just started to modify the electric field as shown in Figs. 2(a) and 2(b). Near the cathode, the field is slightly enhanced while it is somewhat depressed further out. This trend is also predicted by Ogasawara's model of this phase.[19] The negative-ion number density is negligible throughout the discharge.

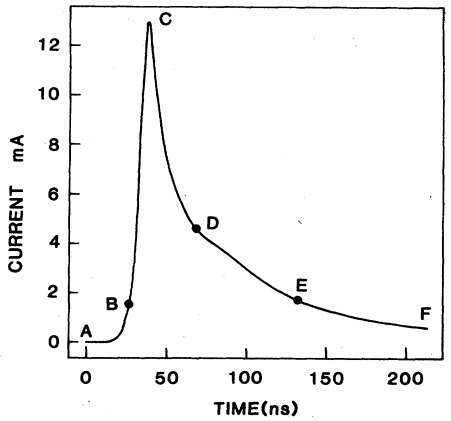

FIG. 1. Computed current in the external circuit vs time for a negative point-plane gap.

At the end of this phase the light output has a weak, diffuse form with a maximum centered at $x=1.7$ mm as shown in Fig. 3. During this phase, the replenishment criterion [Eq. (10)] is strongly satisfied, as shown in Fig. 4, and continuing discharge growth is ensured.

2. Field-collapse phase

During the "field-collapse phase," from $t=26$ to 39 ns (B to C in Fig. 1), the effect of space-charge growth progressively reduces the electric field towards zero in the region of $0.4 \le x \le 1.5$ mm. Through this phase the replenishment-criterion integral [Eq. (10)] declines sharply towards unity, and consequently the current passes through its maximum value. The number of secondary electrons due to photons also rises to a maximum during this phase, while the number of ion secondary electrons is negligible, as shown in Fig. 5. The field near the cathode is enhanced at the same time as the field in region $0.4 \le x \le 1.5$ mm tends to zero and a cathode fall region starts to form. Consequently, we see a movement towards the cathode of the peak in the electron density, positive-ion density, and light output, as shown for $t=35$ ns in Figs. 6(a), 7(a), and 3, respectively. The negative-ion density becomes significant but not dominant at $t=35$ ns [Fig. 8(a)].

3. Cathode sheath formation phase

During the "cathode sheath formation phase," from $t=39$ to 70 ns (C to D in Fig. 1), a well-defined cathode fall region develops and the current decays steadily from its maximum value. The total number of electrons (and positive ions) continues to rise until $t \sim 70$ ns, and as the space-charge control of the electric field intensifies, a well-defined "plasma" develops in the region $0.2 \le x \le 2.0$ mm. The term plasma is used for a quasineutral region which excludes the field from its center[21] [Fig. 2(b)]. The reduction in the field causes the replenishment criterion integral, Eq. (10), to fall below its critical value of unity (Fig. 4). The discharge therefore progressively decays.

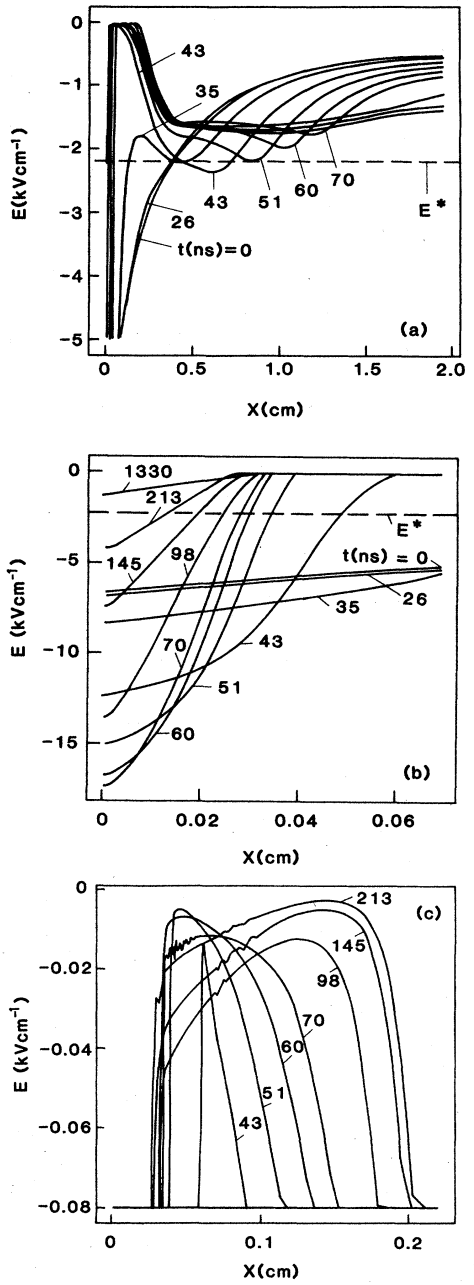

FIG. 2. Electric field vs position at the times shown (ns) after the release of the initial seed electrons. The surface of the sphere electrode is at $x=0$ cm and plane electrode is at $x=2$ cm. E^* is the field at which the ionization coefficient equals the attachment coefficient. (a) Full field distribution from $x=0$ to 2 cm computed with 181 mesh points. (b) The field from $x=0$ to 0.065 cm computed with 100 mesh points. (c) Details of the low-field region expanded between $x=0$ and 0.22 cm to show that $E<0$ everywhere.

Note that the current continues to decay while the electron density continues to rise towards its maximum value (at ~ 70 ns), an effect which reflects the operation of Sato's equation[30] [Eq. (9)].

On the cathode side of the plasma region a cathode fall region develops [Fig. 2(b)], with a strong positive space-charge layer between the plasma and the cathode [Fig. 9(b)]. The cathode fall voltage at $t=70$ ns is 320 V, which is comparable with the cathode fall voltage of 300 V expected for a steady discharge in oxygen.[32] As the cathode fall develops, the high-field region contracts towards the cathode, and hence the region of maximum ionizing activity and light output also moves towards the cathode (Fig. 3).

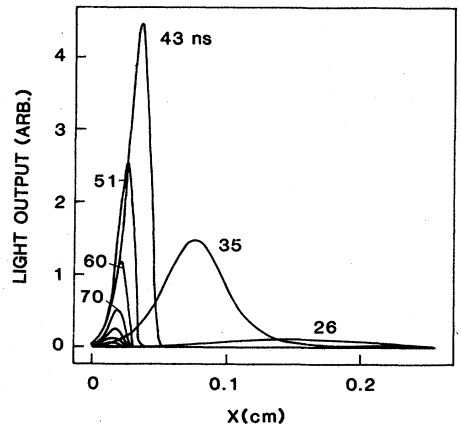

FIG. 3. Light output vs position at various times (ns) after initiation of the calculation for comparison with the results of Ushida *et al.* (Ref. 33).

On the anode side of the plasma region the electric field is also enhanced until $E>E^*$, allowing a net increase in electron numbers, and a weak ionizing wave moves towards the anode[31] [Fig. 2(a)]. At higher voltages this ionizing wave would become an anode-directed streamer and would lead to the breakdown of the gap. At the end of the phase, $t=70$ ns, $E<E^*$ at all positions between the plasma and the anode. In the body of the plasma, the field is low and always negative, as shown in Fig. 2(c). Also note that in Fig. 2(c) at, say $t=70$ ns and $x=0.04$ cm, there is a "wiggle" in the electric field, which reflects

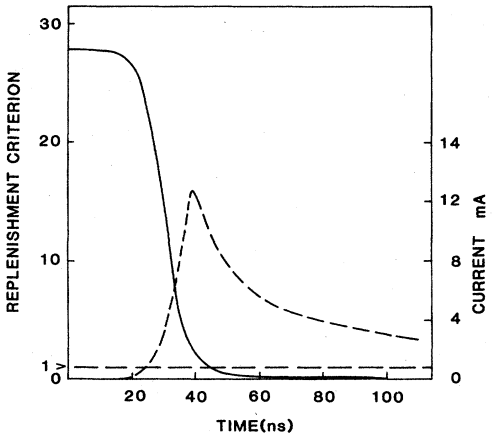

FIG. 4. The replenishment criterion integral [Eq. (10)] and the discharge current vs time, showing the interrelation between the secondary-electron feedback mechanism and the resultant discharge current.

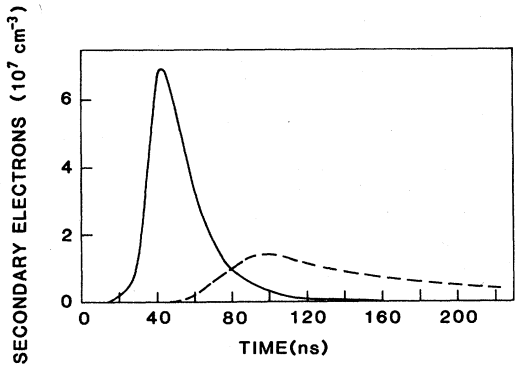

FIG. 5. Number of secondary electrons released at the cathode vs time. Photon secondary electrons, ——; ion secondary electrons, — — —.

a minor numerical instability which does not appear to amplify. Similar corresponding wiggles appear in the electron number-density distribution and charge distributions, shown in Figs. 6(b) and 9(b). Although three-body attachment begins to convert electrons to negative ions, the maximum negative-ion density is still five times smaller than the maximum electron density, and electrons still dominate the discharge.

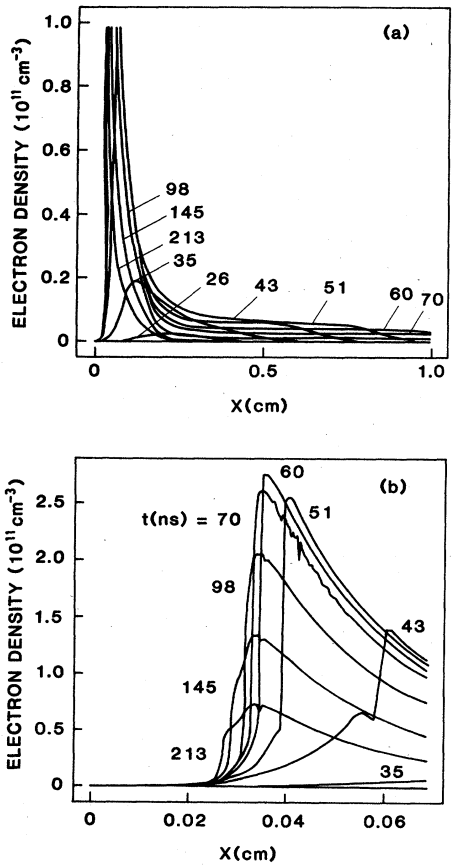

FIG. 6. Electron density vs position at various times. (a) Electron density vs position from $x=0$ to 2 cm using 181 mesh points. (b) Electron density vs position from $x=0$ to 0.065 cm using 100 mesh points.

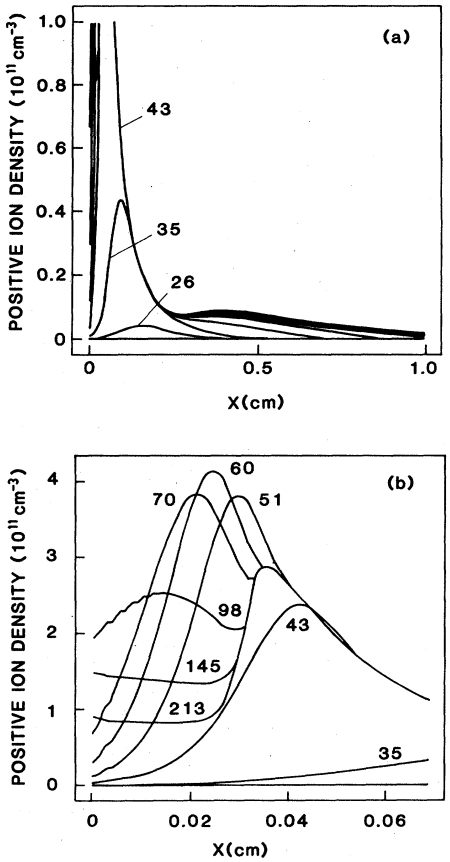

FIG. 7. Positive-ion density vs position at various times. (a) Positive-ion density for the complete gap. (b) Positive-ion density vs position from $x=0$ to 0.065 cm.

4. *Electron removal phase*

During the "electron removal phase," from $t=70$ to 131 ns (Fig. 1, *D* to *E*), electron numbers decline gradually, due to the formation of negative ions, and at the end of this phase the number densities of electrons and negative ions are comparable, as shown in Figs. 6(b) and 8(b). Throughout this time, the cathode fall region adjusts markedly in response to changes in the distribution of positive space charge, but the adjustment has little effect on the discharge behavior. Secondary electrons due to ions become dominant (Fig. 5), but the replenishment criterion integral remains less than unity (Fig. 4) and the discharge continues to decay.

5. *Negative-ion domination phase*

After a time of 131 ns has elapsed (*E* in Fig. 1), the "negative-ion domination phase" begins. The electric field has adopted a configuration in which the replenishment criterion is very much less than unity (Fig. 4). The majority of electrons have been converted to less mobile negative ions [Figs. 6(b) and 8(b)]. Consequently, the discharge continues to decay very slowly.

Although the slow-moving negative ions now control the space-charge distribution, it is the highly mobile electrons which are still the dominant current carrier [Eq.

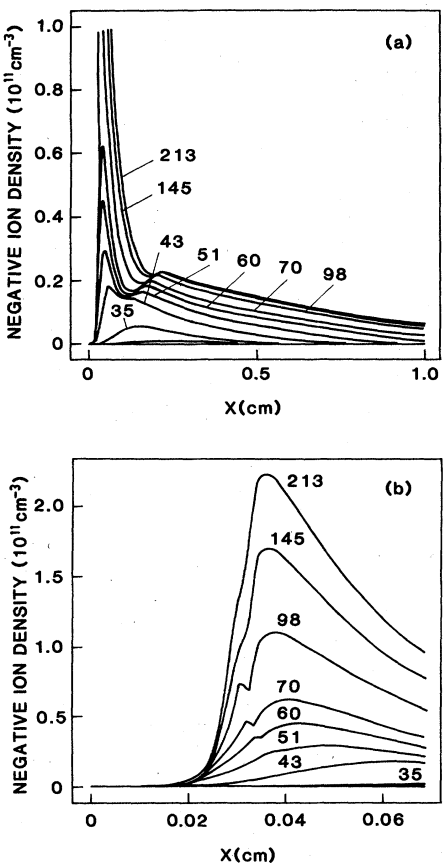

FIG. 8. Negative-ion density vs position at various times. (a) Negative-ion density vs position from $x=0$ to 2 cm using 181 mesh points. (b) Negative-ion density vs position from $x=0$ to 0.65 cm using 100 mesh points.

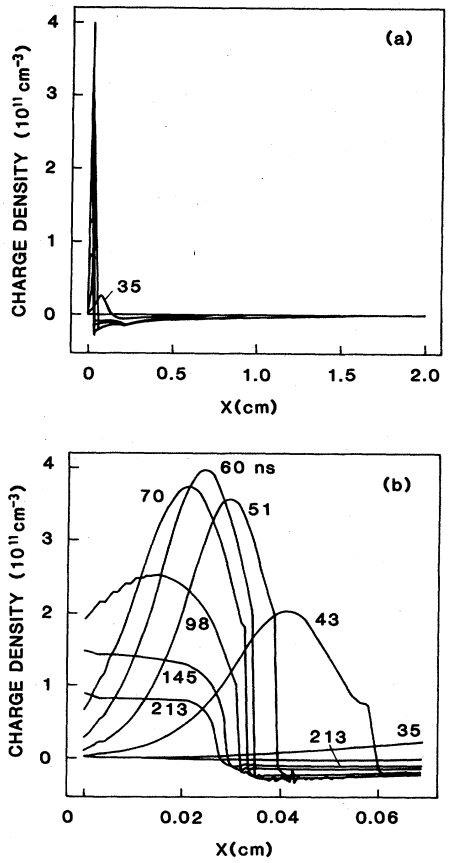

FIG. 9. Net charge density vs position at various times. (a) Charge density over the complete gap. (b) Charge density vs position from $x=0$ to 0.065 cm.

(9)]. It is not until $t=500$ ns that the ions become the dominant current carriers, with positive and negative ions contributing approximately equal components.

Throughout this phase electrons continue to create positive ions between the plasma region and the anode, even though $\alpha \ll \eta$, since α is finite and many electrons reach the anode. These positive ions drift slowly towards the cathode to eventually provide secondary electron seeds for the next Trichel pulse. As shown in Fig. 5, photon secondary electrons dominate early in the pulse, while ion secondary electrons become dominant after $t=80$ ns and continue to contribute electrons at much later times. Thus positive ions can provide the necessary "delayed" replenishment of electrons required to sustain a succession of current pulses.

B. The role of photons in the discharge

Photons are important in the discharge for two reasons; first, they are a source of secondary electrons at the cathode, and second, like the current in the external circuit they are readily observable. Photons may also lead to photoionization and photoexcitation in the gap but these effects have not been considered in this study.

Secondary processes at the cathode are essential for the formation of a self-sustained discharge, as indicated by the replenishment criterion [Eq. (10)] and the discussion of ion secondary electrons. If no secondary processes are included and the calculations repeated, the initial seed electrons form a single avalanche which moves through the gap with no sustained discharge development. However, the presence of secondary electrons due to photoemission leads to a feedback mechanism which sustains the discharge during the current rise and initial quenching phase, as shown in Fig. 5, with ion secondaries playing a role only at later times.

The calculations of light output, presented in Fig. 3, show how the movement of the position of maximum light output towards the cathode reflects the development of the cathode fall region. Figure 10 shows the predicted variation of the position of maximum light output as the discharge develops: the predictions are remarkably similar to the experimental results of Ushita *et al.*,[33] despite the differences in geometry and gas. The apparent velocity of the peak light output, $\sim 5\times 10^6$ cm s^{-1}, and variation in light output amplitude are also similar to the experimental results of Bugge and Sigmond[4,13] and Ushita *et al.*[33]

The movement of the luminous front in this model is similar in some respects to the movement of the light output from cathode-directed streamers in nitrogen, as

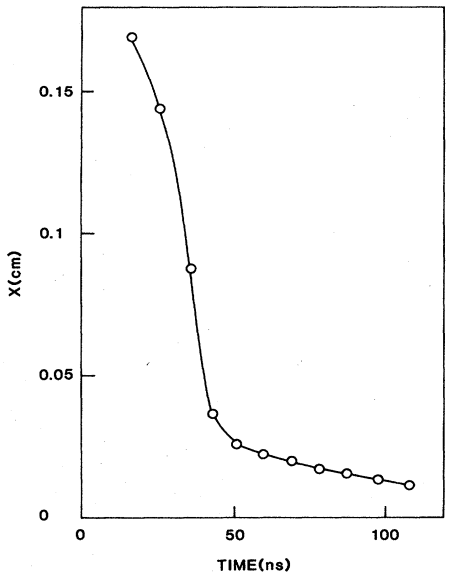

FIG. 10. Position of the point of maximum light output vs time plotted for comparison with the results of Ushida *et al.* (Ref. 33).

described by Davies *et al.*[31] However, in the present case the plasma develops adjacent to the electrode and the light output is associated with the narrowing of the cathode fall region between the plasma and the electrode, whereas the luminous front of a cathode-directed streamer is associated with the propagation of a high-field pulse to the cathode. Thus in the present case the luminous front is not a cathode directed streamer but is strictly a property of the transient cathode sheath formation.

C. The role of attachment in the discharge

To clarify the important role of attachment in the model we have artificially set the attachment coefficients to zero and repeated the calculations. The results are shown in Fig. 11. For the first 40 ns the current waveform matches closely that found in the attaching gas, with a short rise time and a similar rapid initial decay after a peak at ~ 30 ns. The peak pulse height is larger when attachment is absent because of the larger values of net ionization, $\alpha' = \alpha - \eta$. The similarity between the attaching and nonattaching models in the early phases shows that attachment is not important in controlling the pulse rise and its initial decay (see also Davies *et al.*[8]).

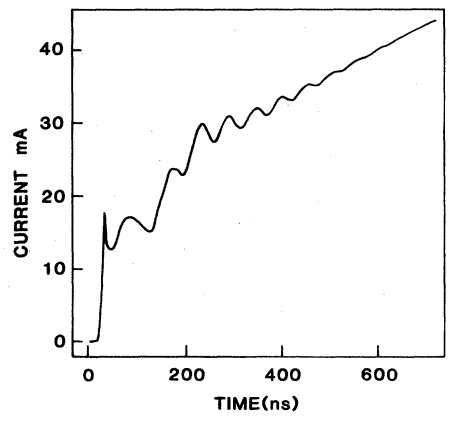

FIG. 11. Computed external circuit current vs time for the same conditions as Fig. 1, but with attachment set equal to zero.

However, in the nonattaching gas the "electron removal phase" does not exist and the electrons move rapidly in response to the initial quenching process. The electron flow results in a current which rises towards a steady value in a series of damped oscillations reflecting the back and forth motion of the electric field in the cathode fall region, as the field attains an equilibrium condition without the damping effect of attachment. A detailed description of the processes of corona onset in nonattaching gases will be the subject of a future paper.

D. The role of diffusion in the discharge

Electron diffusion is most important where the electric field is relatively small and the density gradients steep. These circumstances occur where electrons slow down abruptly in the low-field region after moving through the cathode fall region, such as at $x = 0.3$ mm and $t = 70$ ns in Fig. 6(b). Electrons diffuse towards the cathode due to this steep gradient and attach outside the low-field region to form negative ions. Thus the negative-ion density in the region $0.2 < x < 0.3$ mm, shown in Fig. 8(b), is larger than the electron density in that region, while elsewhere the negative-ion density still lags behind the electron density. When the diffusion is set to zero electrons do not move back towards the cathode and at $t = 70$ ns the negative-ion density is everywhere less than the electron density; also the current amplitude is reduced by 10%, but otherwise the current pulse shape and all other variables are very similar. Diffusion therefore does not have a dominant effect, although for fine grid spacings it does seriously limit the time step via Eq. (13).

IV. DISCUSSION

This section draws together the ideas presented above to develop a general picture of the mechanism of pulse formation in negative corona. The discussion centers around two observable quantities, the external circuit current and the light output.

The current pulse discussed in Sec. III is the "first" Trichel pulse in that, unlike subsequent pulses, the discharge occurs in a region initially free of space charges. The initial rapid rise in the current is due entirely to electrons in the undistorted high-field region near the point cathode. A large number of electrons with high velocity are produced by ionization, giving a large current, according to Eq. (9). The rapid current rise is not due to field enhancement at the cathode, as postulated by Dancer *et al.*,[18] as this field enhancement largely occurs during the initial current decay.

It is of interest to examine the mechanisms for the rise and fall of the current in the Trichel pulse. The transit time for electrons over the sheath distance of the order of 0.04 cm is approximately 1 ns. This time is small compared with the time to maximum pulse current of 40 ns,

so that the electron-density distribution near the cathode after 1 ns is approximately given by $N_e(x) = N_e(x=0)\exp(\alpha x)$. The increase in current then depends on the variation in time of $N_e(x=0)$ at the boundary rather than being given by $N_e(x,t) = N_e(x,0)\exp(\alpha W t)$.

This process is quite unlike a simple avalanche mechanism because the feedback due to photoemission and the nonuniform electric field ensure that the rapid growth of electron numbers is concentrated in the region near the cathode. Thus although in principle Aleksandrov's[6] multiple avalanche mechanism is embodied in our continuity equations we need not consider the concept of a single-electron avalanche in our theory.

There are a number of possible mechanisms for the decay in current after the pulse maximum at 40 ns.

(a) Electrons could convert to negative ions as postulated by Loeb.[1] But at 40 ns electrons are still the dominant negative particle by an order of magnitude, see Figs. 6(b) and 8(b).

(b) The principal electrons could move from the high-field region near the point to the lower-field region away from the point where they form negative ions, thus reducing the current, with negligible space-charge field distortion. We believe that this is the reason for the decay in the current pulse of Davies and Donne.[8]

(c) Positive ions could be absorbed by the cathode and reduce the space-charge field near the cathode and thus the current. This mechanism was postulated by Dancer *et al.*[18] and indeed contributes to the current decay in our calculations after 70 ns. But before 40 ns, the positive ions have only moved ~ 0.005 cm.

(d) The width of the cathode sheath can be reduced and the field beyond the cathode sheath brought close to zero by space-charge effects so that the replenishment criterion is not satisfied; i.e., an electron from the cathode is not replaced by secondary emission effects during its transit across the electrode space. (Note also that the majority of electrons are immobilized in the low-field region.) It is this mechanism which was postulated by Trichel[2] and is the reason for the decay of current in our calculations after 39 ns, see Figs. 2(b) and 4.

Thus in summary the current is quenched and decays because a dense plasma, which may be termed a "negative-glow" region, is formed and excludes the electric field from its center. Between the plasma and the cathode, positive ions dominate the space charge to form a prominent but narrow cathode sheath. The discharge is then quenched because the replenishment criterion is not satisfied. (Eventually $E < E^*$ everywhere and no net increase in electron density is possible.) The entire rise and initial decay of the current pulse can therefore be viewed as a process involving the formation of a transient cathode sheath.

During the rise and initial fall of the current, electrons dominate the current flow and electrons and positive ions dominate the space-charge distribution. However, as the current continues to decline, attachment leads to the formation of negative ions, and these dominate the space-charge distribution after ~ 131 ns. Thus the electron—positive-ion plasma is converted into a plasma of positive and negative ions. The low mobility of both kinds of charge carrier then "freezes" the electric field in this "switched-off" state.

The movement of the position of maximum light output towards the cathode is related to the development of the cathode sheath. The maximum light output follows the contraction of the high-field region towards the cathode.

The computed current in the external circuit (Fig. 1) shows a typical Trichel-pulse shape very similar to that measured by Bugge[13] in oxygen at 50 Torr with a small radius cathode. The rise time of 11 ns and pulse width of 50 ns correspond well with the measurements of Bugge.[13] The maximum current of 13 mA is larger than Bugge's measurements, as expected for a larger-diameter point and also for the *first* Trichel pulse compared with subsequent pulses which occur in the presence of space charge from the previous pulses.

V. CONCLUSIONS

We have demonstrated many of the principal mechanisms responsible for the formation of negative corona pulses in an electronegative gas. The current pulse shape and light output history are adequately explained. The theory explains the current pulse rise and decay in terms of the time-dependent formation of a cathode sheath region. The theory has emphasized the importance of the relatively wide "plasma" region which brings the electric field close to zero over much of the cathode region. The theory has also demonstrated the crucial role played by attachment in converting electrons to negative ions, freezing the electric field formation in place. Although previous theories have hinted at these features, they have never been the subject of rigorous computation.

Three-body attachment at low-field strengths plays an important role in the model, and it is clearly important to know this parameter accurately for calculations of this type. Since the rate of three-body attachment is pressure dependent, a study of pulsed corona discharges at different pressures could be very instructive.

It is shown that diffusion plays only a minor role in current pulse formation. The replenishment criterion is found to be a useful simple tool in understanding the different phases of the discharge and in predicting corona onset voltages.

The importance of adequately resolving all of the cathode phenomena in order to adequately describe the current pulses is clearly shown. It is necessary to use a variable mesh of points to resolve the cathode region, because of the finite number of points possible within computers. The variable-mesh "flux-corrected-transport" (FCT) algorithm has proved very accurate and stable for this difficult problem.

ACKNOWLEDGMENTS

Doctor J. J. Lowke provided the guidance, inspiration, advice, and support which made this project possible. I would particularly like to acknowledge the support and advice of Dr. L. E. Cram during the course of this work

and his help in preparing this manuscript. I would also like to acknowledge discussions with the following people: Dr. P. Bayle, Professor, H. A. Blevin, Dr. D. L. Book, Dr. P. Chantry, Dr. O. Farish, Dr. J. H. Ingold, Dr. A. V. Phelps, Dr. N. Sato, and Professor H. Tagashira.

APPENDIX A: PRESCRIPTION OF THE TRANSPORT COEFFICIENTS

The calculations are performed using the material properties of oxygen at a pressure of 6.67 kPa (50 Torr), presented here in SI units. The ionization and two-body attachment coefficients were taken from Hake and Phelps[34] and Frommhold[35] and represented as functions of E/N as follows:

$$\alpha/N = 2.124\times10^{-20}\exp(-6.2116\times10^{-19}N/E)\ \mathrm{m}^2\ . \tag{A1}$$

The two-body attachment coefficient η_2 was given by

$$\eta_2/N = 2.0\times10^{-22}m^2 \quad \text{for } E/N > 1.835\times10^{-20}\ \mathrm{V\,m}^2\ , \tag{A2}$$

and

$$\eta_2/N = 5.032\times10^{30}\,(E/N)^{2.655}\ \mathrm{m}^2 \quad \text{for } E/N < 1.835\times10^{-20}\ \mathrm{V\,m}^2\ . \tag{A3}$$

An expression for the rate coefficient for three-body attachment K_{a3} was developed from the data of Chanin *et al.*,[36] Grunberg,[37] Rees,[38] Nelson *et al.*,[39] and Pack *et al.*[40] by Phelps:[41]

$$K_{a3} = \left[\frac{3.0\times10^{-42}}{1+[(E/N)/4.0\times10^{-21}]^{3/2}}\right]\mathrm{m}^6\,\mathrm{s}^{-1}\ . \tag{A4}$$

This yields a three-body attachment coefficient per unit length η_3 as follows:

$$\eta_3 = N^2K_{a3}/|W_e|\ . \tag{A5}$$

The two- and three-body attachment coefficients may be combined to give a net coefficient

$$\eta = \eta_2+\eta_3\ . \tag{A6}$$

The recombination coefficient β is taken to be the same for ion-ion recombination as for electron-ion recombination

$$\beta = 2.0\times10^{-13}\ \mathrm{m}^3\,\mathrm{s}^{-1}\ . \tag{A7}$$

The electron-diffusion coefficient is based on the survey of electron-swarm data by Dutton[42] and is represented as follows: for $E/N < 2.0\times10^{-21}\ \mathrm{V\,m}^2$,

$$D/\mu_e = 1.343\times10^{6}(E/N)^{0.3441}\ \mathrm{V}\ , \tag{A8}$$

and for $2\times10^{-21} < E/N < 1.23\times10^{-20}\ \mathrm{V\,m}^2$,

$$D/\mu_e = 1.213\times10^{25}(E/N)^{1.2601}\ \mathrm{V}\ , \tag{A9}$$

while for $E/N > 1.23\times10^{-20}\ \mathrm{V\,m}^2$,

$$D/\mu_e = 1.519\times10^{9}(E/N)^{0.461\,13}\ \mathrm{V}\ , \tag{A10}$$

where μ_e is the electron mobility.

The mobilities μ_i of the positive and negative ions are assumed to be equal and given by[43]

$$\mu_i = 5.5\times10^{21}(1/N)\ \mathrm{v}^{-1}\,\mathrm{s}^{-1}\,\mathrm{m}^2\ . \tag{A11}$$

The electron drift velocity is taken from the data of Hake and Phelps[34] and Frommhold[35] and is represented by

$$W_e = 5.747\times10^{16}(E/N)^{0.6064}\ \mathrm{m\,s}^{-1}\ . \tag{A12}$$

Secondary emission processes are included by assuming one excited state with a lifetime of $\tau = 10^{-8}$ s, efficiency of emission $\gamma = 10^{-3}$, and absorption range $\mu = 0\ \mathrm{m}^{-1}$. The ion secondary ionization coefficient γ_i was estimated from the work of von Engel[44] as $\gamma_i = 0.01$.

APPENDIX B: ADDITIONAL STABILITY CRITERIA

An extensive account of the methods used in this study has been given by Morrow and Cram.[23,24] The following additional points were found to be important when the electric field approaches zero due to space-charge effects and also at the boundary.

(1) The FCT algorithm uses drift velocities $w_{i+1/2}$ evaluated at points $x_{i+1/2}$ lying midway between mesh points. These velocities must be obtained using the value of the electric field $E_{i+1/2}$ computed at the midpoints. The operator which implements Eq. (4) can be constructed to yield the required field values.

(2) For stability and accuracy it is necessary to solve the equations, including the source terms, using a method which is second order in time. Intermediate solutions are computed half a time step ahead, $t+\Delta t/2$, then using source terms and velocities computed at $t+\Delta t/2$ the solution is advanced a full time step from t to $t+\Delta t$.

(3) At absorbing boundaries, for both positive and negative ions, the particle densities are not prescribed and must be computed self-consistently. In the body of the discharge the Phoenical "low-phase error" Shasta algorithm is used.[23,24] This is matched at the boundary to give the flux into the boundary point using the simple explicit Shasta algorithm.[23] Specifically we compute the flux from the last grid point into the electrode using

$$\Delta N = -\frac{\Delta t N_B W_{\mathrm{ex}}}{\Delta x_B}$$

where N_B is the density at the boundary and Δx_B is the grid spacing at the boundary. W_{ex} is the particle velocity linearly extrapolated from values within the plasma to give a fictitious value at half a grid space beyond the boundary.

APPENDIX C: VARIABLE MESH DISTRIBUTION

The variable mesh is defined along the axis of symmetry of the electrode system as the set

$$x_i = x_{i-1}+\delta x_i \quad (i=2,3,\ldots,181)\ , \tag{C1}$$

with the surface of the spherical cathode at $x=0$ cm. It is found that a very fine-mesh resolution of $\delta x_i = 4.17\ \mu\mathrm{m}$ is required in the region $3.0\times10^{-2} \le x_i \le 4.5\times10^{-2}$ cm, $(i=38,39,\ldots,72)$, where the net charge reverses sign and the electric field tends to zero. In the high-field region

near the cathode, $x_i < 3\times10^{-2}$ cm, this fine mesh would unnecessarily limit the time step via Eq. (12); thus a coarser mesh is used initially with $\delta x_2 = 14.55$ μm, contracting towards the fine-mesh region using $\delta x_i = 0.9649\delta x_{i-1}$ ($i=3,4,\ldots,37$). On the anode side of the fine-mesh region the mesh is steadly expanded using $\delta x_i = 1.0523\delta x_{i-1}$ ($i=73,74,\ldots,181$), until $\delta x_{181} = 0.103$ cm and $x_{181} = 2.0$ cm.

[1]L. B. Loeb, *Electrical Coronas* (University of California, Berkeley, 1965).

[2]G. W. Trichel, Phys. Rev. **54**, 1078 (1938).

[3]R. J. Van Brunt and D. Leep, J. Appl. Phys. **52**, 6588 (1981).

[4]R. S. Sigmond, in *Electrical Breakdown of Gases,* edited by J. M. Meek and J. D. Craggs (Wiley, New York, 1978), pp. 319—384.

[5]M. Goldman and A. Goldman, in *Gaseous Electronics,* edited by M. Hirsh and H. J. Oskam (Academic, New York, 1978), Vol. 1, Chap. 4, p. 219.

[6]G. N. Aleksandrov, Zh. Tekh. Fiz. **33**, 223 (1963) [Sov. Phys.—Tech. Phys. **8**, 161 (1963)].

[7]D. Graf, *Proceedings of Sixth International Conference on Gas Discharges, Edinburgh, 1980,* edited by B. F. Hampton (Institute of Electrical Engineers, London, 1980), pp. 142—145.

[8]A. J. Davies and K. E. Donne, in Ref. 7, pp. 138—141.

[9]R. Morrow and J. J. Lowke, in *Proceedings of the Seventh International Conference on Gas Discharges, London, 1982,* edited by O. Farish (Institute of Electrical Engineers, London, 1982), pp. 124—127.

[10]L. B. Loeb, J. Appl. Phys. **19**, 883 (1948).

[11]L. B. Loeb, J. Phys. Rev. **86**, 256 (1952).

[12]R. Zentner, Z. Angew. Phys. **29**, 294 (1970).

[13]C. Bugge, Technical Report No. EIP 68-1, Norwegian Institute of Technology, 1969 (unpublished).

[14]C. Bugge and R. S. Sigmond, in Proceedings of the Ninth International Conference on Phenomena in Ionized Gases, Bucharest, 1969 (unpublished), p. 289.

[15]M. Khalifa and M. Abdel-Salam, *Third International Conference on Gas Discharges, London, 1974,* edited by D. J. Tedford (Institute of Electrical Engineers, London, 1974), pp. 311—314.

[16]L. C. Thanh, Proc. Inst. Electr. Eng. **126**, 270 (1979).

[17]M. M. Kekez, P. Savic, and G. D. Lougheed, J. Phys. D **15**, 1963 (1982).

[18]P. Dancer, R. C. Davidson, O. Farish, and M. Goldman, *IEEE—IAS Annual Meeting,* Cleveland, Ohio, 1979 (IEEE Industry Applications Society, Cleveland, 1979), pp. 87—90, Library of Congress No. 73-647500.

[19]M. Ogasawara, J. Phys. Soc. Jpn. **21**, 2360 (1966).

[20]P. S. Gardiner, J. L. Moruzzi, and J. D. Craggs, J. Phys. D **11**, 237 (1978).

[21]R. Morrow and J. J. Lowke, J. Phys. D **14**, 2027 (1981).

[22]R. Morrow, J. Comput. Phys. **46**, 454 (1982).

[23]R. Morrow and L. E. Cram, in *Computational Techniques and Applications,* edited by J. Noye and C. H. J. Fletcher (North-Holland, Amsterdam, 1984), pp. 719—730.

[24]R. Morrow and L. E. Cram, J. Comput. Phys. **57**, 129 (1985).

[25]J. J. Lowke and D. K. Davies, J. Appl. Phys. **48**, 4991 (1977).

[26]A. J. Davies and C. J. Evan, Proc. Inst. Electr. Eng. **114**, 1547 (1967).

[27]A. J. Davies, C. J. Evans, and F. Llewellyn-Jones, Proc. R. Soc. London Ser. A **281**, 164 (1964).

[28]L. V. Bewley, *Two-Dimensional Fields in Electrical Engineering* (Macmillan, New York, 1948).

[29]I. Abbas and P. Bayle, J. Phys. D **13**, 1055 (1980).

[30]N. Sato, J. Phys. D **13**, L3 (1980).

[31]A. J. Davies, C. S. Davies, and C. J. Evans, Proc. Inst. Electr. Eng. **118**, 816 (1971).

[32]J. D. Cobine, *Gaseous Conductors* (Dover, New York, 1958).

[33]T. Ushita, N. Ikuta, and M. Yatsuzuka, Bull. Fac. Eng., Tokushima Univ. **4**, 89 (1967).

[34]R. D. Hake and A. V. Phelps, Phys. Rev. **158**, 70 (1967).

[35]L. Frommhold, Fortschr. Phys. **12**, 597 (1964).

[36]L. M. Chanin, A. V. Phelps, and M. A. Biondi, Phys. Rev. Lett. **2**, 344 (1959).

[37]R. Grunberg, Z. Naturforsh. **24**, 1039 (1969).

[38]J. A. Rees, Aust. J. Phys. **18**, 41 (1965).

[39]D. R. Nelson and F. J. Davies, J. Chem. Phys. **57**, 4079 (1972).

[40]J. Pack and A. V. Phelps, J. Chem. Phys. **44**, 1870 (1966).

[41]A. V. Phelps (private communication).

[42]J. Dutton, J. Chem. Ref. Data **4**, 577 (1975).

[43]L. Harrison and J. L. Moruzzi, J. Phys. D **5**, 1239 (1972).

[44]A. von Engel, *Ionized Gases* (Oxford University, London, 1965).